International Journal of Thermal Sciences 131 (2018) 14–19

Contents lists available at ScienceDirect

International Journal of Thermal Sciences

journal homepage: www.elsevier.com/locate/ijts

Design and realization of thermal camouflage with many-particle systems

Ruizhe Wang[a], Jin Shang[a], Jiping Huang[a,b,*]

[a] Department of Physics, State Key Laboratory of Surface Physics, Key Laboratory of Micro and Nano Photonic Structures (MOE), Fudan University, Shanghai 200433, China

[b] Collaborative Innovation Center of Advanced Microstructures, Nanjing 210093, China

ARTICLE INFO

Keywords:
Heat conduction
Camouflage
Sensor-misleading
Many-particle structure

ABSTRACT

An object can be found and identified by detecting its scattering signature of various physical fields, e.g., electromagnetics, acoustics, thermotics, etc. Similar to optical illusion, a thermal camouflage device can replace an expected object without altering the heat scattering pattern. Here, we propose and realize a two-dimensional metasurface, which is capable of controlling the heat flow and can be used as a device for misleading thermal sensors. The thermal metasurface is composed of conventional particles with many-body local-field effects. Our experiments and finite-element simulations have confirmed the thermal camouflage effect for both line and point heat sources, demonstrating the performance of thermal illusion. Also, we show that this many-particle structure can be extended to three-dimensional systems, which opens a door for designing applicable camouflage devices in the future.

1. Introduction

Controlling various physical fields, including optics [1–3], electromagnetics [4–6], magnetics [7,8], acoustics [6,9,10], etc., is highly desired for the design of field manipulation devices. Among all these fields control devices, thermal metamaterial [11,12,14–19,21–27] has recently stimulated great interest due to the important role it played in thermotics devices design. Along with rapid development of artificial technology, many thermal metamaterials with novel thermal properties have been experimentally demonstrated, such as invisibility cloaks [11–17] (which are used to let heat flow around an object as if the object does not exist), thermal concentrators [18–20] (which are used to concentrate heat into a specific region) and rotators [19,21] (which are used to rotate the flow of heat as if it comes from a different angle).

Instead of invisibility cloaks that can change an expected object into nothing, a thermal camouflage device [23–27] can replace an object A by using special designed structures of an object B without changing heat flux pattern. Recently, there has been a surge of attention focused on the designs of thermal camouflage devices, including Laplace-equation-based devices [23,24] which can exhibit thermal illusions not only in a steady state but also in a transient state, transformation-optics-based devices [25,26], and camouflaging devices in multiphysical fields [27]. However, for the former design of camouflage devices, unconventional material parameters are required to experimentally realize thermal camouflage. Namely, the parameters of the materials have to satisfy either the singularity in the bilayer-cloak designs or inhomogeneity in the coordinate-transformation designs.

In this paper, we report a thermal camouflage device based on many-body local-fields effect, which can simulate the thermal scattering signature of an expected object in the environment. In contrast to the previous designs which require unconventional material properties, our many-particle metasurface is composed of conventional particles based on naturally occurring materials. In an actual experimental setup, the proposed device is carefully examined for both line and point heat/cold sources by inserting thermal sensors, demonstrating an excellent sensor misleading performance. Furthermore, three-dimensional simulated results show that this structure can be extended to practical camouflage device.

The function of many-particle structure and its realization of sensors misleading are schematically illustrated in Fig. 1. A speaker exposed in a thermal conduction field can be detected by three thermal sensors because of the thermal conductivity difference between the speaker and the background environment. However, when the speaker is replaced by a many-particle structure with well-designed effective thermal conductivity, the thermal properties of the speaker can be simulated by the many-particle structure, and able to provide three thermal sensors the same thermal signature of the speaker. Therefore, the thermal sensors which are given a thermal signature of an expected object can be 'deceived' by precisely designed many-particle camouflage structure.

* Corresponding author. Department of Physics, State Key Laboratory of Surface Physics, Key Laboratory of Micro and Nano Photonic Structures (MOE), Fudan University, Shanghai 200433, China.
E-mail address: jphuang@fudan.edu.cn (J. Huang).

https://doi.org/10.1016/j.ijthermalsci.2018.05.027
Received 8 October 2017; Received in revised form 10 May 2018; Accepted 16 May 2018

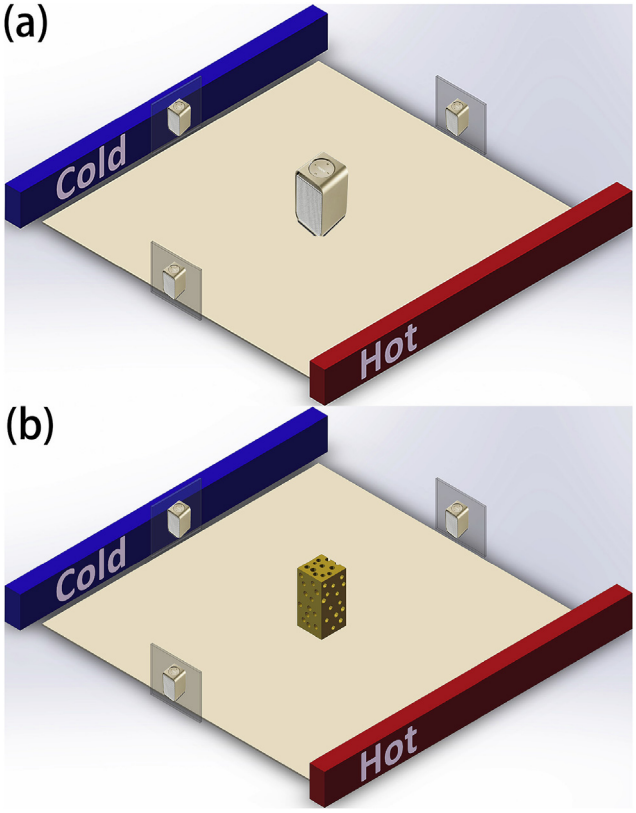

Fig. 1. Schematic illustration of the thermal sensor misleading device: (a) Three thermal sensors can detect a speaker in the heat conduction field; (b) Well designed many-particle device can "deceive" thermal sensors by providing them the same thermal signature of the speaker.

2. Theory

We consider two simple two-dimensional square systems. In the first system [Sample I in Fig. 2], n kinds of circular particles, each with thermal conductivity κ_i and area fraction p_i ($i = 1, ..., n$), occupy the whole central square region with a random distribution (the many-particle structure). Four small square areas, which are placed around the central square region with thermal conductivity κ_d, play the role of thermal detectors, and the environment background is occupied by a material with thermal conductivity κ_b. For comparison, in the second system [Sample II in Fig. 2], the central square region is replaced by a uniform material serving as an expected object with thermal conductivity κ_o , and the same thermal detectors and environment background with that of first system are used. In the presence of an external temperature gradient, if the temperature distribution or heat flows at the detectors for two systems are the same, the many-particle structure is considered to be a sensor-misleading device. For this purpose, it is necessary to set the many-particle structure to possess an effective thermal conductivity κ_e that must be equal to κ_o .

For a single circular particle with thermal conductivity κ_i , area fraction p_i and radius R embedded in a uniform two-dimensional host with effective thermal conductivity κ_e, the solution of the Laplace's equation in polar coordinates (r,θ) is

$$T_{\text{inner}}(r, \theta) = a_0 + b_0\ln(r) + \sum_{m=1}^{\infty}[a_m\cos(m\theta) + b_m\sin(m\theta)]r^m + \sum_{m=1}^{\infty}[c_m\cos(m\theta) + d_m\sin(m\theta)]r^{-m},$$

$$T_{\text{outer}}(r, \theta) = a'_0 + b'_0\ln(r) + \sum_{m=1}^{\infty}[a'_m\cos(m\theta) + b'_m\sin(m\theta)]r^m + \sum_{m=1}^{\infty}[c'_m\cos(m\theta) + d'_m\sin(m\theta)]r^{-m},$$

where $T_{\text{inner}}(r, \theta)$ and $T_{\text{outer}}(r, \theta)$ denote the distribution of temperature in the particle and the host, respectively. Here a_0, b_0, a_m, b_m, c_m, d_m, a'_0, b'_0, a'_m, b'_m, c'_m, and d'_m are undetermined coefficients. The accompanying boundary conditions are

$$T_{\text{inner}}(r = 0) < \infty,$$

$$T_{\text{outer}}(r \to \infty, \theta) \to T_0 + C\, r\cos(\theta),$$

$$T_{\text{inner}}(r = R) = T_{\text{outer}}(r = R),$$

$$\kappa_e \frac{\partial T_{\text{outer}}}{\partial r}\bigg|_{r=R} = \kappa_i \frac{\partial T_{\text{inner}}}{\partial r}\bigg|_{r=R},$$

Here T_0 denotes the temperature at $r = 0$, C is a constant depending on applied temperature gradient. Thus, we can obtain the temperature

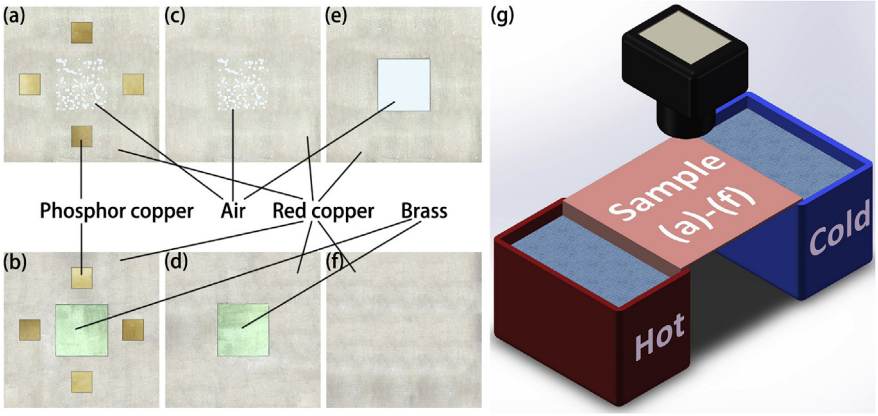

Fig. 2. (a–f) Experimental samples I-VI and (g,h) experimental setup. (a–f) show a 20 cm×20 cm system, which owns a central square area (6.7 cm×6.7 cm). Brass (b,d) with thermal conductivity 148 W/(m·K) is serving as an expected object. For (a,c) the many-particle structure, the central square area contains air particles of thermal conductivity 0.026 W/(m·K) and area fraction 31.03% randomly embedded in red copper of 390 W/(m·K) and 68.97%; the red copper can be seen as an assembly of circular particles with different sizes; outside the central square area is the background environment also occupied by red copper. Four small phosphor copper square areas in (a,b) with 54 W/(m·K) play the role of thermal detectors. (For interpretation of the references to colour in this figure legend, the reader is referred to the Web version of this article.)

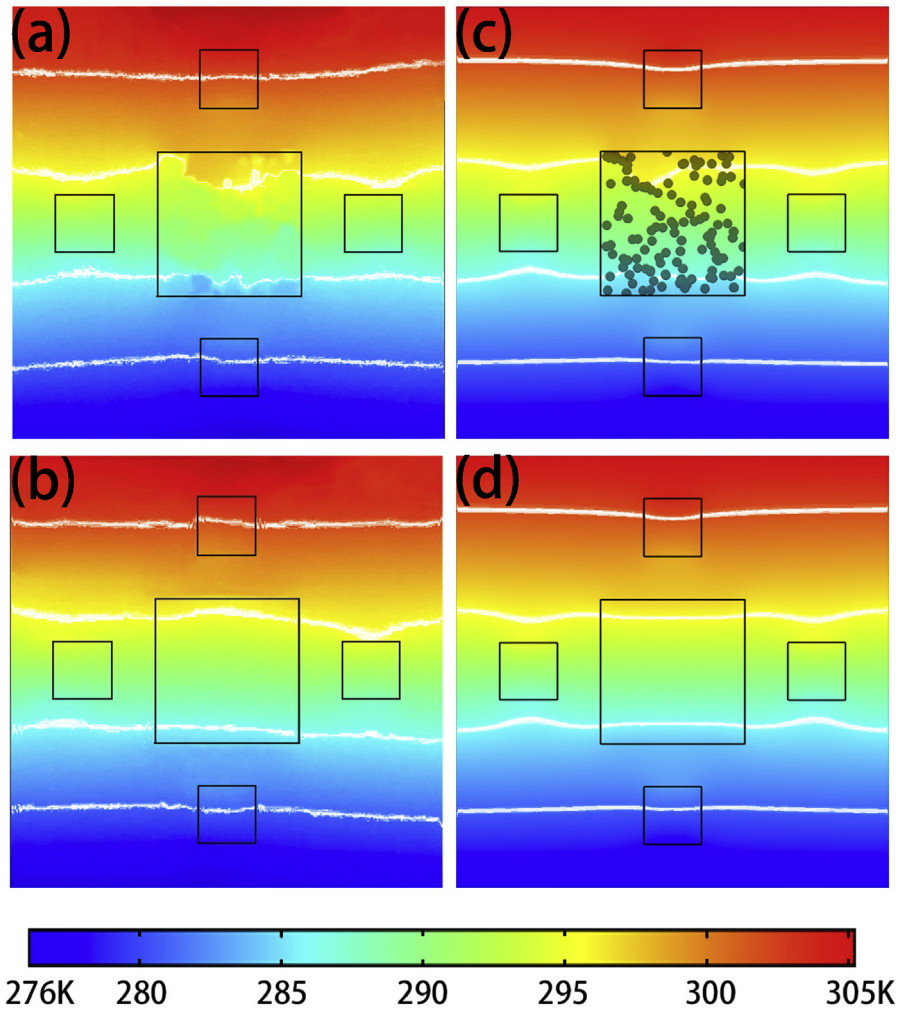

Fig. 3. Temperature-distribution comparison between (a,b) experimental results of Samples I-II in Fig. 2 and (c,d) corresponding simulated results for line heat/cold sources: (a,c) many-particle structure and (b,d) expected object, and the white lines are isotherms.

distribution inside and outside the circular particle:

$$T_{\text{inner}}(r,\theta) = T_0 - \frac{2\kappa_i}{\kappa_i+\kappa_e} C\, r\cos\theta,$$

$$T_{\text{outer}}(r,\theta) = T_0 + C\, r\cos\theta - \frac{\kappa_i-\kappa_e}{\kappa_i+\kappa_e} C\, R^2\frac{\cos(\theta)}{r}. \tag{3}$$

Then, we can write the Clausius-Mossotti factor β_i as

$$\beta_i = \frac{\kappa_i-\kappa_e}{\kappa_i+\kappa_e}, \tag{4}$$

which describes the degree of thermal contrast between the circular particle and the host. Clearly, $\beta_i = 0$ corresponds to zero thermal contrast, i.e., the particle and the host share the same material. Thus, when the thermal contrasts of all the particles within the central square area can be cancelled out, that is

$$\sum_{i=1}^{N} p_i\cdot\beta_i = 0, \tag{5}$$

the many-particle structure [Fig. 2(a)] will provide an effective thermal conductivity κ_e which can be equal to that of the expected object in the second system [Fig. 2(b)] by carefully designing the area fraction of each particle. Therefore, this many-body local-field effect can lead to a sensor misleading phenomenon as the temperature distribution of many-particle structure and expected object are the same at the sensors.

2.1. Experiment and simulation

For simplicity, we consider the case that the many-particle metasurface is composed of two materials with thermal conductivity κ_1 and κ_2. κ_1 is much smaller than κ_b, which contributes to expelling heat flux lines and attracting isotherms while κ_2 is equal to κ_b which does not distort the heat flux lines and isotherms. Thus, with the contribution of two materials at certain area fractions, the sensor misleading phenomenon can be achieved by providing an effective thermal conductivity κ_e ($\kappa_1 < \kappa_e < \kappa_2 = \kappa_b$) which is equal to κ_o according to Equation (5). The four small square areas with thermal conductivity κ_d which play the role of thermal detectors are placed around the many-particle structure [Sample I in Fig. 2]. For comparison, the many-particle structure is replaced by a uniform central square area with thermal conductivity κ_o serving as an expected object [Sample II in Fig. 2].

In order to examine the above theoretical deduction, experiments are firstly carried out to verify the performance of thermal camouflage in both line and point shaped heat/cold sources. The experimental samples and setup are depicted in Fig. 2. All the experimental samples are manufactured by chemical etching, and 0.1 mm-thick polydimethylsiloxane films are covered on the samples in order to eliminate the infrared reflection. Two water tanks which are filled with hot water and ice water serve as line heat and cold sources, respectively. Temperature-tunable electric heating rod sticking at the back of the sample is used for a point heat source. The room temperature is tuned to the

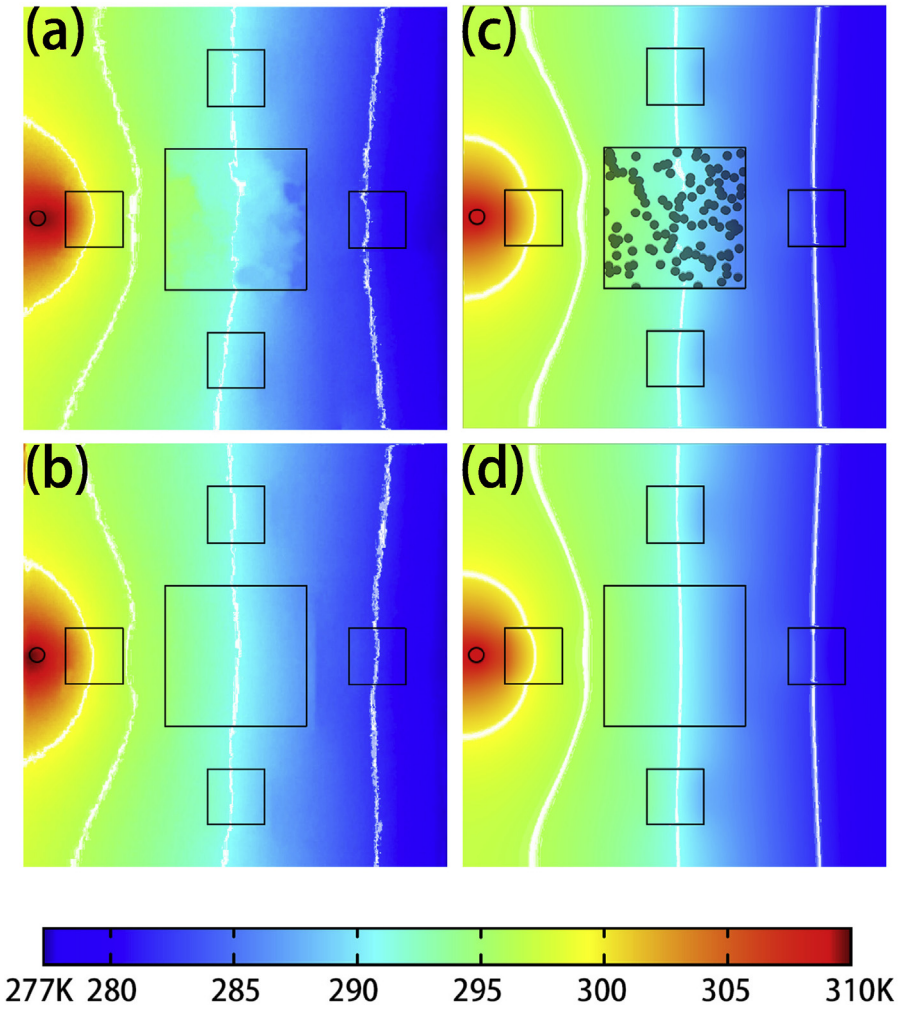

Fig. 4. Same as Fig. 3, but for point heat sources.

middle temperature of heat and cold source which can minimize the thermal convection towards air. The temperature distribution at the sample is measured by using infrared camera (Flir E60). Commercial software Matlab is used to plot relevant experimental data which not only shows the line heat source [Fig. 3(a,b)] but also the point heat source [Fig. 4(a,b)]. Since the thermal contact resistance of the welded junctions (which connect different materials) and thermal convection affect the performance of the samples, the isotherms of experimental samples are not as smooth as simulation ones. However, the performances of thermal are still satisfactory for both line and point shaped heat/cold sources.

We further perform finite-element simulations to confirm the above experimental results. All the parameters used in the simulations are the same with that used in the above experiments. Besides, the air convection is considered in the simulation, and the air convection coefficient h is set to be $5\,W/(m^2{\cdot}K)$. Fig. 3(c,d) and Fig. 4(c,d) show the finite-element simulations based on the commercial software COMSOL Multiphysics which agree well with the above experiments. So far, both experiments and simulations confirm that the many-particle structure can ”deceive” the thermal sensors providing them a thermal illusion of an expected object. The many-particle metasurface is composed of two materials, but the temperature distribution for these two pure materials are entirely different from the many-particle metasurface [see Fig. 5(e,g,h)]. Hence, the realization of thermal camouflage is not solely determined by one material but many-body local-field effect. Fig. 5(e,f) clearly shows that the temperature distribution in the environment without detector of many-particle system is nearly equivalent to that of expected object system. Experimental results [Fig. 5(a–d)] acquired based on sample III-VI in Fig. 2 are consistent with simulated results in Fig. 5(e–h).

Furthermore, we extend this many-particle structure to three-dimensional system, where finite-element simulation has been applied to study two cubic systems. Fig. 6 shows that by precisely controlling the effective thermal conductivity of many-particle structure in the center of the cube, the temperature distribution and heat flux arrow in the background environment of these two cubic systems are the same. Hence, we estimate that the sensor misleading can also be achieved in the presence of thermal detectors in the background environment of these two cubes. The three-dimensional simulated results can give the prediction that our many-particle structure can be applied to future practical sensor misleading device.

3. Conclusion

In summary, by developing an effective medium theory, we have demonstrated a many-particle thermal metasurface which can be used as a camouflage device. The agreement between experiment and simulation shows that a notable sensor misleading phenomenon has been achieved for both line and point heat sources. For simplicity, Our device is composed of two materials. However, based on many-body local-field effect, we can always design a multi-material composed many-particle camouflage device which greatly widen the applicability of this

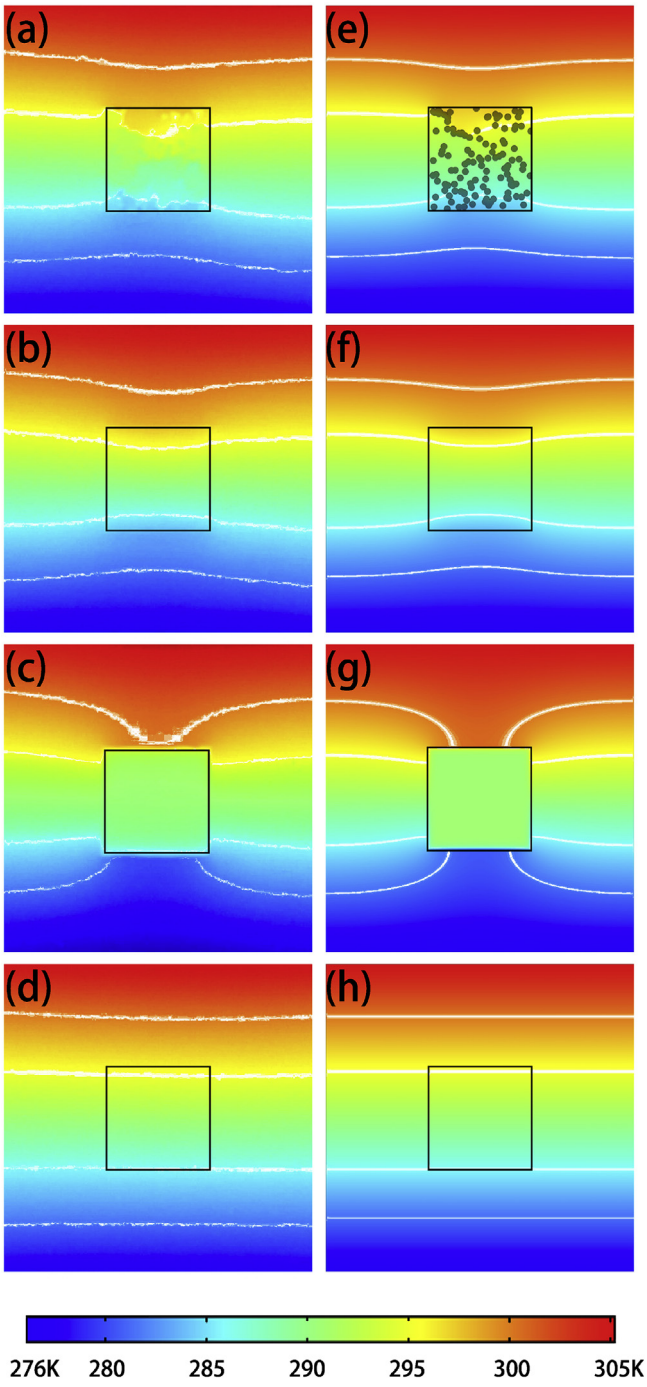

Fig. 5. Temperature-distribution comparison between (a–d) experimental results of Samples III-VI in Fig. 2 and (e–h) corresponding simulated results in the absence of detectors: (a,e) many-particle structure and (b,f) expected object. Also, we show the results of two pure materials which are used to compose the many-particle structure: (c,g) air and (d,h) red copper. (For interpretation of the references to colour in this figure legend, the reader is referred to the Web version of this article.)

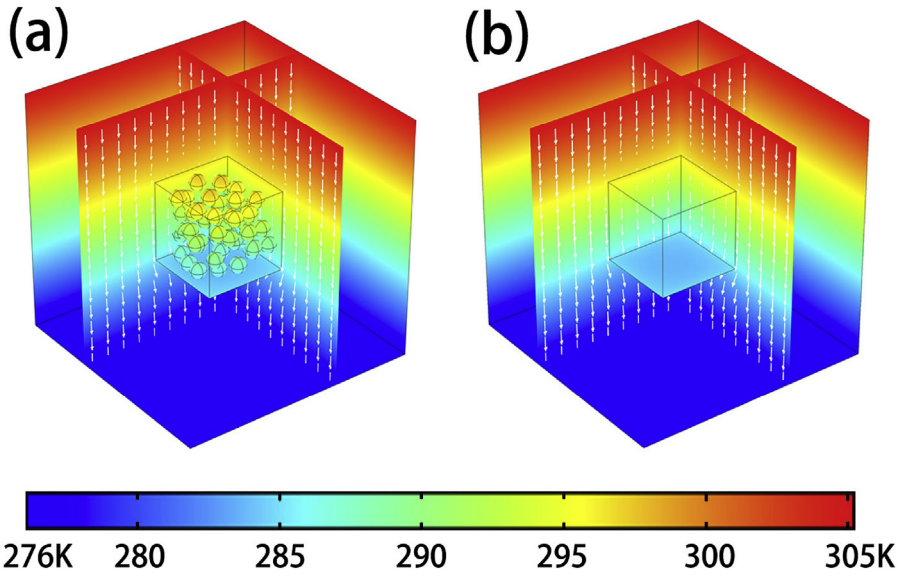

Fig. 6. Three-dimensional finite-element simulation of temperature distribution: (a) many-particle structure and (b) expected object. The arrows denote the heat flux. In (a) the many-particle structure, the central cubic volume contains fifty air particles with thermal conductivity 0.026 W/(m·K) and volume fraction 41.37% randomly embedded in red copper with 390 W/(m·K) and 58.63%; outside the central cubic volume is the background environment with 109 W/(m·K). In (b), brass [148 W/(m·K)] serves as an expected object occupying the central cubic volume. (For interpretation of the references to colour in this figure legend, the reader is referred to the Web version of this article.)

structure. Three-dimensional simulations have also been performed for the structure, which may be more practical and commercially available in future camouflage device design.

Acknowledgments

We are grateful to Mr. L. J. Xu and Mr. C. R. Jiang for their useful discussions. We acknowledge the financial support by the National Natural Science Foundation of China under Grant No. 11725521, and by the Science and Technology Commission of Shanghai Municipality under Grant No. 16ZR1445100.

References

[1] U. Leonhardt, Optical conformal mapping, Science 312 (2006) 1777–1780.
[2] V.M. Shalaev, Transforming light, Science 322 (2008) 384–386.
[3] H.Y. Chen, C.T. Chan, P. Sheng, Transformation optics and metamaterials, Nat Mater 9 (2010) 387–396.
[4] J.B. Pendry, D. Schurig, D.R. Smith, Controlling electromagnetic fields, Science 312 (2006) 1780–1782.
[5] D. Schurig, J.J. Mock, B.J. Justice, S.A. Cummer, J.B. Pendry, A.F. Starr, et al., Metamaterial electromagnetic cloak at microwave frequencies, Science 314 (2006) 977–980.
[6] A. Greenleaf, Y. Kurylev, M. Lassas, U. Leonhardt, G. Uhlmann, Cloaked electromagnetic, acoustic, and quantum amplifiers via transformation optics, Proc Natl Acad Sci 109 (2012) 10169–10174.
[7] F. Gömöry, M. Solovyov, J. Šouc, C. Navau, J.P. Camps, A. Sanchez, Experimental realization of a magnetic cloak, Science 335 (2012) 1466–1468.
[8] J.F. Zhu, W. Jiang, Y.C. Liu, G. Yin, J. Yuan, S.L. He, et al., Three-dimensional magnetic cloak working from d.c. to 250 kHz, Nat Commun 6 (2015) 8931–8931.
[9] H.Y. Chen, C.T. Chan, Acoustic cloaking in three dimensions using acoustic metamaterials, Appl Phys Lett 91 (2007) 183518–183518.
[10] L. Zigoneanu, B.I. Popa, S.A. Cummer, Three-dimensional broadband omnidirectional acoustic ground cloak, Nat Mater 13 (2014) 352–355.
[11] C.Z. Fan, Y. Gao, J.P. Huang, Shaped graded materials with an apparent negative thermal conductivity, Appl Phys Lett 92 (2008) 251907–251907.
[12] U. Leonhardt, Cloaking of heat, Nature 498 (2013) 440–441.
[13] M. Maldovan, Sound and heat revolutions in phononics, Nature 503 (2013) 209–217.
[14] R. Schittny, M. Kadic, S. Guenneau, M. Wegener, Experiments on transformation thermodynamics: molding the flow of heat, Phys Rev Lett 110 (2013) 195901–195901.
[15] H.Y. Xu, X.H. Shi, F. Gao, H.D. Sun, B.L. Zhang, Ultrathin three-dimensional thermal cloak, Phys Rev Lett 112 (2014) 054301–054301.
[16] T.C. Han, X. Bai, D.L. Gao, T.L. Thong, B.W. Li, C.W. Qiu, Experimental demonstration of a bilayer thermal cloak, Phys Rev Lett 112 (2014) 054302–054302.
[17] Y.G. Ma, Y.C. Liu, M. Raza, Y.D. Wang, S.L. He, Experimental demonstration of a multiphysics cloak: manipulating heat flux and electric current simultaneously, Phys Rev Lett 113 (2014) 205501–205501.
[18] S. Guenneau, C. Amra, D. Veynante, Transformation thermodynamics: cloaking and concentrating heat flux, Optic Express 20 (2012) 8207–8218.
[19] S. Narayana, Y. Sato, Heat flux manipulation with engineered thermal materials, Phys Rev Lett 108 (2012) 214303–214303.
[20] F.J. Arias, On the use of thermal conductive focusing for solar concentration enhancement, Int J Therm Sci 108 (2016) 17–27.
[21] S. Guenneau, C. Amra, Anisotropic conductivity rotates heat fluxes in transient regimes, Optic Express 21 (2013) 6578–6583.
[22] X.Y. Shen, J.P. Huang, Thermally hiding an object inside a cloak with feeling, Int J Heat Mass Tran 78 (2014) 1–6.
[23] T.C. Han, X. Bai, T.L. Thong, B.W. Li, C.W. Qiu, Full control and manipulation of heat signatures: cloaking, camouflage and thermal metamaterials, Adv Mater 26 (2014) 1731–1734.
[24] T.Z. Yang, Y. Su, W. Xu, X.D. Yang, Transient thermal camouflage and heat signature control, Appl Phys Lett 109 (2016) 121905–121905.
[25] Y.X. Chen, X.Y. Shen, J.P. Huang, Engineering the accurate distortion of an object¡¯s temperature-distribution signature, Eur Phys J Appl Phys 70 (2015) 20901–20901.
[26] N.Q. Zhu, X.Y. Shen, J.P. Huang, Converting the patterns of local heat flux via thermal illusion device, AIP Adv 5 (2015) 053401–053401.
[27] T.Z. Yang, X. Bai, D.L. Gao, L.Z. Wu, B.W. Li, T.L. Thong, et al., Invisible sensors: simultaneous sensing and camouflaging in multiphysical fields, Adv Mater 27 (2015) 7752–7758.